Chapter 3

Experimental Techniques and Procedures

3.1 Introduction

This chapter describes the experimental techniques and procedures used to characterize the jet flow and the propulsive performance of the vehicle. Section 3.2 describes the features of the facility where the experiments were conducted. The remainder of the chapter is divided into two main sections. Section 3.3 describes the techniques used for experiments in which the vehicle was held in a stationary position and section 3.4 describes the experimental techniques used during the measurements of self-propulsion. Data acquisition during the stationary experiments was relatively simple, as described in section 3.3.1. Two techniques were used to characterize the jet flow. Digital particle image velocimetry is discussed in section 3.3.2 and planar laser-induced fluorescence is described in section 3.3.3. The data acquisition in the self-propelled experiments is described in section 3.4.1. As the vehicle propels down the facility, a motorized traverse was designed to follow the vehicle at a preset distance using a control system as discussed in section 3.4.3. Two experimental techniques were used for the investigation of propulsive performance. Laser Doppler velocimetry was used to obtain measurements of the jet flow as described in section 3.4.4 and drag measurements were used in the estimation of the total hydrodynamic efficiency. The details for the drag experimental procedure are found in section 3.4.5.

3.2 Test Facility

The experiments were conducted in a 40 m tilting water tunnel and wave generation facility in the Keck Laboratory at the California Institute of Technology. The tunnel has a cross-sectional area of 110 cm in width and 60 cm in height. Figure 3.1(a) is an image of the upstream view of the facility. The submarine was designed to be positioned in the center of the tunnel. The long length of the tunnel allowed sufficient run time for the self-propulsion experiments. This facility is equipped with a controllable motorized traverse that translates along the flume rails. A schematic of the traverse can be viewed in figure 3.2. The traverse was used to hold necessary equipment for experiments. In addition to controlling speed, the direction of translation can also be set by a control panel in the center of the facility. Software was developed to control the speed of the motorized traverse via a computer (section 3.4.3) and record the position and speed of the motorized traverse that is displayed on the control panel (section 3.4.3). See figure 3.1(b) for an image of the control panel.

(a) Image of the upstream view of the 40 m water tunnel facility.

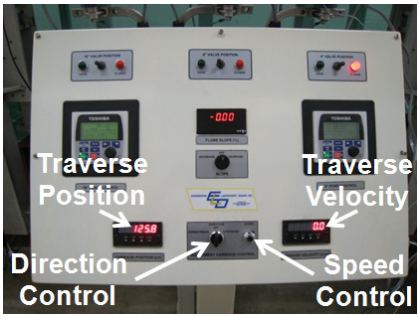

(b) Image of the panel used to control the direction and speed of the motorized traverse.

Figure 3.1. Images of facility and control panel for motorized traverse.

3.3 Measurement Techniques and Applications (Stationary Configuration)

3.3.1 Data-Acquisition System

The initial voltage supplied to the vehicle by a battery was measured using a digital multimeter (Fluke). The current flow into the system was measured by placing a current clamp (Fluke) on one of the power leads to the motor batteries. The output of the current clamp was connected to a digital multimeter and the average display value was recorded. The usable current range of the current clamp is 0.5 to 1000 amps. The accuracy of the device is 2.0% of the reading +/- 0.5 amps. The motor speed was measured by connecting the output from the tachometer to a hand-held tachometer reader (Monarch). This device allowed the motor speed to be displayed and the average value to be recorded.

3.3.2 Digital Particle Image Velocimetry Measurements

Digital particle image velocimetry (DPIV) is a technique for obtaining flow field measurements (Willert and Gharib 1991). A thin laser sheet illuminates a particle-seeded flow. A camera, perpendicular to the laser sheet, records images as the particles are illuminated. By cross-correlating intensity fields in a subsection of two successive images, an average displacement of the particles in the sampling window can be calculated. This procedure is repeated across the image area, generating the flow displacement field between the time at which the two images were taken. Dividing the flow displacement field by the time difference between the two images yields the velocity field of the flow.

Particles used to seed the flow for experiments were neutrally buoyant, silver-coated, hollow glass spheres with a 13 μm diameter and density of 1.6 g/cm^3 (Potters Industries). Plastic barriers were used to confine a 30 m section, eliminating the need to fill the entire tunnel with particles. The particles were illuminated by two Nd:YAG lasers (New Wave) with a power rating of 30 mJ per pulse at a 532 nm wavelength. The laser beam is collimated by a cylindrical lens and then reflected

by a mirror to illuminate a cross-section of the jet. See figure 3.2.

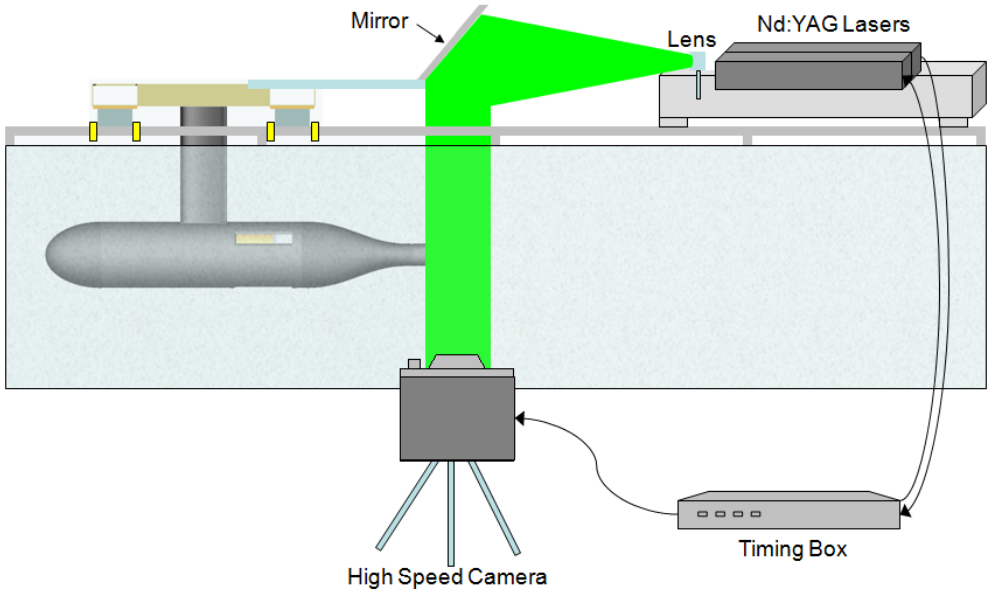

Figure 3.2. Schematic of DPIV setup for the jet flow of the vehicle in a stationary configuration.

The laser and optics are mounted in a stationary position on the motorized traverse. Since the pulsing frequency of the lasers is fixed at 15 Hz, one laser is pulsed at preset time delay to allow for greater measurement resolution. A schematic diagram of the laser pulsing is shown in figure 3.3. One laser is used as a master and sends a +5 V TTL pulse to a custom timing box when the Q-switch laser is energized. The timing box then sends a +5 V TTL pulse to trigger the second laser and camera at preset time delays. Varying the time delay to the second laser is used to set the timing between images. A Photron high speed camera is set to random reset trigger mode with a frame speed of 60 fps and a frame size of 1024×1024 pixels. The time difference between images was varied from 5.31 ms to 21.17 ms. Either a 60 mm or 105 mm lens was used with the camera depending on the field of view desired.

After postprocessing images from initial experiments, many errant vectors resulted. This error was attributed to particles moving in and out of the laser sheet. Honeycomb was placed in the exit of the jet nozzle to remove swirl from the propeller. The honeycomb was 2.0 inches in length and 2.0 inches in diameter, with a 0.125 inch diameter cell size. The honeycomb increased the pressure loss in the nozzle leading to significant thrust reduction. For this reason, it was removed during

experiments involving self-propulsion.

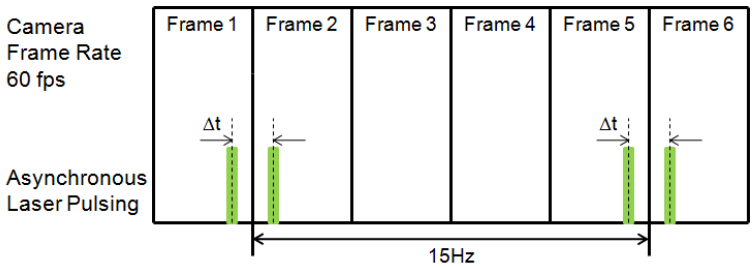

Figure 3.3. Schematic diagram of camera frame rate and laser pulsing.

Processing of the DPIV images was accomplished using an in-house developed code. Generally two approaches were taken depending on the field of view. For the steady jet results, shown in section 4.3.1, the 60 mm lens was used. Postprocessing of this data used a 32×32 pixel sampling window and a 16×16 step size. These parameters produced accurate vector fields with few or no errant vectors per image. For the unsteady shell geometries, a 105 mm lens was used to increase spatial resolution. This field of view encompassed only half the jet diameter. For these sets of images, a sampling window of 64×64 pixels with a 32×32 step size was used. Once it was evident that the unsteady shell geometry was producing fluid roll up, the 60 mm lens was used to verify symmetric fluid roll up otherwise known as vortex ring formation.

3.3.3 Planar Laser-Induced Fluorescence Measurements

Planar laser-induced fluorescence (PLIF) is a technique widely used for flow visualization and for quantitative measurements (Smits and Lim 2000). PLIF was used for flow visualization for the results shown in section 4.3.2. A 60 mm lens was used for imaging, providing a field of view with the spatial resolution of 3 jet diameters in the axial direction and 1.3 jet diameters in radial direction. One difference between DPIV and PLIF is in the medium that is used for illumination. In PLIF, the fluid medium is either comprised of fluorescent material or can be seeded with a fluorescent particulate substance. Rhodamine 6G, a fluorescent dye with maximum absorption wavelength of 530 nm was injected in the fluid housing by a syringe through tygon tubing. Dye was continuously injected imposing negligible momentum to fluid passing through the submarine inlet until sufficient data was

captured. In addition to the Rhodamine dye, the particles present from the DPIV experiments also absorbed the laser light. A deep golden amber filter (Lee Filter), allowing light transmission from 550 to 700 nm, was placed over the camera lens to block out the DPIV particle emission but accept the rhodamine dye fluorescence.

3.4 Measurement Techniques and Applications (Self-Propelled Configuration)

3.4.1 Data Acquisition System

An electrical box provides signal conditioning, sensor power, and submarine power switching. The electrical box is composed of an aluminum housing containing a bread board, sensor power supply and power shunt resistor. Submarine motor power interconnects use 12-gauge wire, while sensor power or data interconnects use 26-gauge wire. The electrical box provides two 9-pin D-subminiature connections. One is an input for submarine telemetry from the submarine and related sensors, while the second is an output of submarine telemetry to the data acquisition box. The electrical box also provides two screw-type Molex connectors. One is an input from the submarine motor power supply, while the second is the submarine motor power output to the submarine. The sensor power supply cord is also routed to the electrical box.

Due to voltage input limitations of +/- 10 V on the data acquisition box, it is necessary to condition the submarine motor voltage measurement before supplying the signal to the data acquisition box. It is also not possible to measure the voltage across the submarine motor directly as this leads to a large common-mode voltage in the measured signal. This is an artifact of the submarine speed controller design. To avoid the common-mode component, the voltage is measured independently, with respect to power supply ground, at the positive and negative side of the submarine motor. The differences between these two measurements is computed in software and results in the effective voltage across the submarine motor. Even with this scheme, it is still necessary to voltage divide the measured signals down to within input limits of the data acquisition box. This is accomplished

through two similar voltage dividing circuits mounted on the electrical box breadboard. Each circuit consists of two 1/4 watt, 5% tolerance resistors of values 15 and 50 KΩ which are connected in series. The circuit output voltage is read across the smaller resistor giving a circuit gain of 0.23 +/- 0.02. This provides the capability of reading submarine motor voltages of over 40V based on data acquisition box input limits. See Appendix C for a wiring diagram of the electrical box.

The electrical box powers the submarine tachometer and traverse distance sensor. These devices require 5 V power. This is provided by the internal Acopian power supply. The Acopian power supply is rated at 0.5 A and packaged in a fully enclosed plastic case with screw-type connectors. It requires standard 110 VAC facility power via a three-prong power plug.

A thermal breaker switch mounted to the surface of the electrical box serves not only as an on-off switch for submarine motor power but also as a safety device. The breaker is rated for a current of 35 A. In addition, the negative submarine motor power line is routed to an internal 0.01 Ω shunt resistor. The voltage drop across the shunt resistor is used to calculate the submarine motor power supply current. The shunt resistor is capable of dissipating the heat generated by the submarine motor current through a built-in heat sink as well as the electrical box housing.

Submarine and sensor telemetry, except for the submarine motor current, is routed via the electrical box to a National Instruments multifunction data acquisition box. The data acquisition box is responsible for sampling and digitizing telemetry voltages for use in software. It also generates the motorized traverse drive signal discussed in section 3.4.3. The data acquisition box analog inputs and outputs operate on 0 to 10 V signals. While the data acquisition box is capable of measuring an aggregate 250K samples per second for all channels, software processing restricts the sampling rate to approximately 400 Hz.

Submarine motor current is measured via a current clamp (Fluke). The current clamp is attached to the negative line of the submarine power cable between the submarine and the speed controller. This location was chosen in order to avoid including the speed controller's internal current draw in the submarine motor current measurement. The current clamp produces a 1 mV per current amp signal +/- 2.0% of the reading +/- 0.5 A. It is zeroed prior to submarine power on via its adjustment

knob.

In order to capture the current clamp signal, it was necessary to use a device with a greater sampling rate than provided by the data acquisition box. The submarine speed controller introduces high-frequency components in the submarine motor current due to its voltage chopping mechanism. These high frequency components would lead to aliasing of the signal when measured using the data acquisition box. The Data Physics SignalCalc ACE dynamic signal analyzer was used for this task as it provides a 204.8 KHz sample rate and 24-bit measurement resolution. The signal analyzer consists of a portable, USB powered measurement device, known as Quattro, and a data analysis software suite. A software option was purchased that allows continuous logging of measurements to disk.

3.4.2 Data Acquisition Software

The main telemetry application is the Submarine data acquisition (DAQ). The Submarine DAQ is responsible for the collection, calibration and logging of submarine telemetry as well as the transmission of the motorized traverse control drive signal. This software was implemented in LabVIEW 8.5 on a Windows XP platform and consists of a single top level virtual instrument, or VI, and two sub-VIs. One script contains the application's state machine. Another is used to apply a calibration curve to the raw distance sensor output to convert from volts to centimeters. A third applies a linear moving average to the power supply current, motor voltage, and distance sensor signals to filter out high frequency noise.

The Submarine DAQ user interface is broken down into four areas as shown in figure 3.4. The Telemetry area displays the telemetry sample rate as well as charts submarine telemetry including power supply current, submarine motor voltage, the submarine tachometer output and the distance sensor output. The log area allows the enabling and disabling of the telemetry logging function as well as the location and name of the current log file. The Analog Output area displays and allows the enabling or disabling of the motorized traverse drive signal. Finally a Start button situated in the lower-right corner is used to start the application.

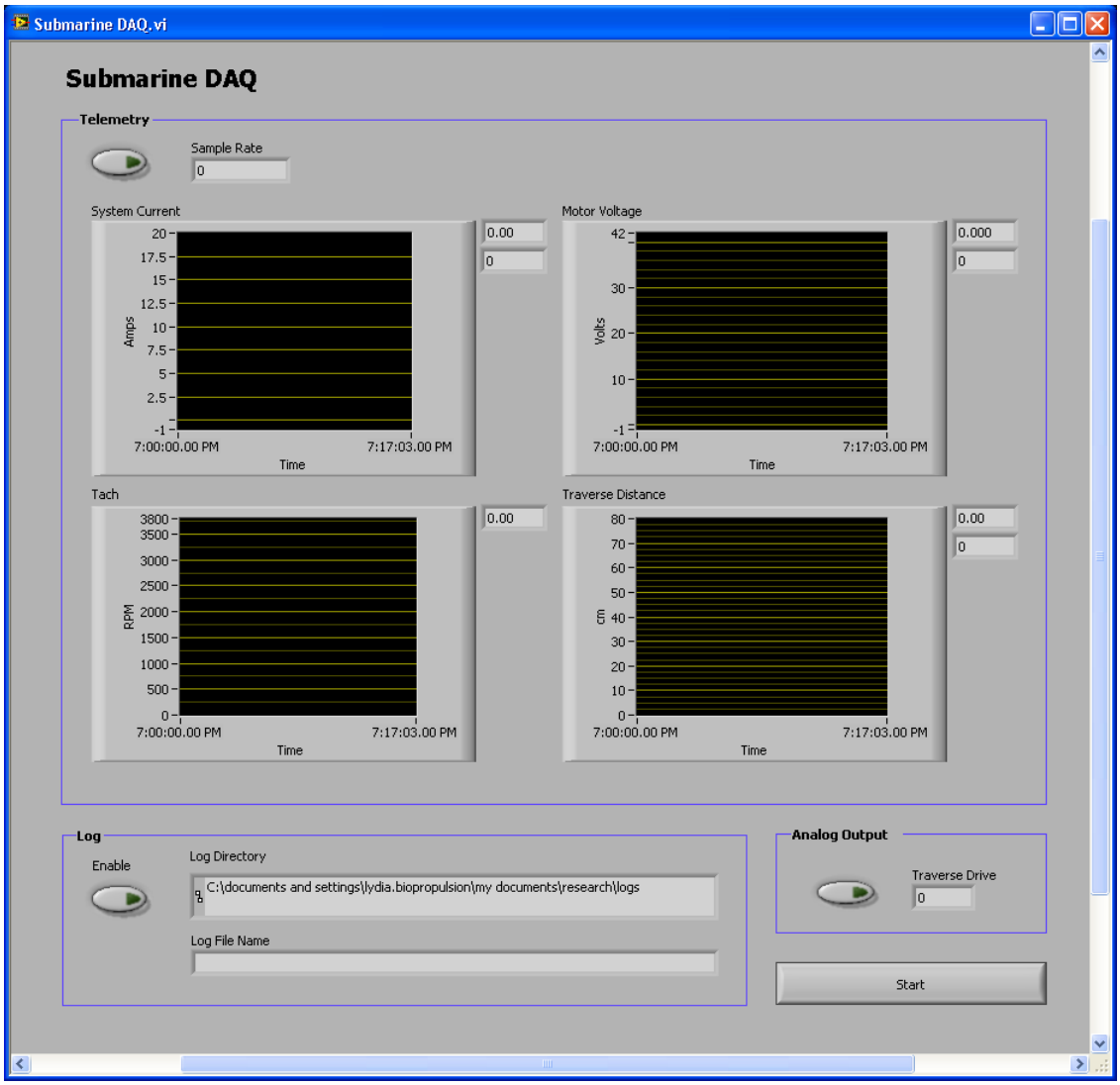

Figure 3.4. Screenshot of Submarine DAQ user interface.

The DAQ VI design consists of a single state machine depicted in the flow chart in Appendix A. Execution begins at the Initialize state. Here the application state is reset and user interface elements are populated with default values. Execution then continues to a wait state. In this state the user interface is monitored until the user clicks on the Start button. Once the Start button is selected, the state machine moves into its main control loop.

The first state in the Submarine DAQ main control loop checks if the user has selected the Stop button. If this is not the case, the control flows to the Measure state. In the Measure state, each of the signals that are connected to the data acquisition box is sampled. The measured signals are

then calibrated in the Calibrate state. Here each measured analog voltage is converted into the desired engineering units. For voltage or current measurements, this is a linear conversion with a single multiplying value. For the distance sensor output, a polynomial calibration curve is applied to convert the signal into centimeters. The tachometer output is a special case as it is a digital signal. The tachometer outputs a square wave whose frequency is proportional to the rotation speed of the motor shaft. In order to derive the signals frequency, the signal is processed using a power spectrum. The peak value of this power spectrum corresponds to the signal's digital frequency. This frequency is in turn used to derive the rotation speed of the motor shaft. At this point, the distance sensor output is also transmitted to the motorized traverse control software via a shared variable. The next state is the Control state. Here a motorized traverse drive value is received from the traverse control software. If enabled, the motorized traverse drive value is output from the data acquisition box. The next two states, Log and Display, perform the described operations. In the event that a log file is not already open upon entering the Log state, the OpenLog state is called which opens a new log file. Execution then moves back to the beginning of the main control loop. If at this point, the user has selected the Stop button, control continues to the Stop state.

The Stop state is responsible for closing an open log file if it exists. Upon completion of this state, the Submarine DAQ software returns to the Wait state where it will remain idle until the user has once again selected the Start button. The Submarine DAQ software produces TDMS formatted binary log files. This is an NI controlled format. This format was chosen as opposed to ASCII text logs as it reduces CPU utilization during logging operations and produces smaller file sizes. The TDMS files may be read from LabVIEW using built in VIs or optionally imported into Excel via an Excel add-in available from the NI website.

3.4.2.1 Motorized Traverse Telemetry

Motorized traverse position and velocity are provided from the motorized traverse control panel over an RS-232 serial interface with an RJ11 connector. The interface protocol uses a 9600 baud rate, eight bit bytes, one stop bit and no parity. To simplify connection to modern workstations, an

RS-232 to USB converter is used for each data channel. This allows direct connection to a computer USB port. The motorized traverse decimal measurements are encoded as ASCII text with carriage return delimiters and transmitted consecutively over the serial interface.

The Traverse Monitor software reads, displays and logs the motorized traverse position and velocity. The Traverse Monitor was implemented in Microsoft Visual C++ 2008 on a Windows XP platform. It connects to one or two serial ports over which the motorized traverse telemetry is received. An initialization file is required as input to the application and one or more log files are produced if logging is enabled.

The Traverse Monitor user interface contains a Telemetry and Options section as shown in figure 3.5. The Telemetry section displays the current motorized traverse position and velocity. The Options section allows the position or velocity channel to be disabled if one is not being used and also enables logging. The bottom of the user interface has a Start and Stop button. The user must select the desired options before selecting the Start button. The Stop button is only made available once the application has started.

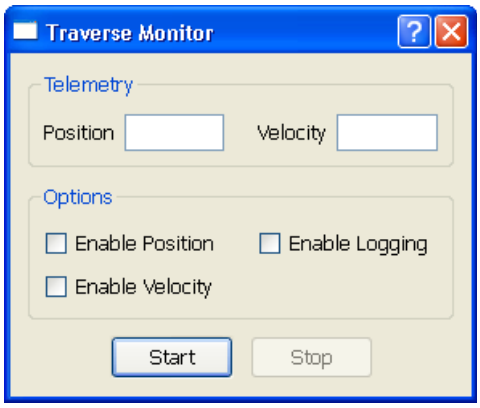

Figure 3.5. Screenshot of Traverse Monitor user interface.

The Traverse Monitor begins execution by reading in the initialization file. The initialization file contains serial port identifiers, display and logging options. Once the initialization file is read, a log file is opened if necessary. Logs contain time stamped measurements in an ASCII text, comma-delimited format. One or two threads are then started depending on whether position, velocity or both channels are enabled. Each thread opens its corresponding serial port and moves into a loop.

The first operation in the loop is to check if the user has stopped the application. If this is not the case, ASCII text data is read from the serial port. This data is then appended to a buffer. The buffer is subsequently searched for stream delimiters which denote the end of a complete measurement. If a delimiter is found, the measurement is extracted, logged and displayed. This sequence of steps continues indefinitely until the user stops the application. The final operation of each thread after the Stop button has been selected is the closing of its corresponding serial port.

3.4.2.2 Distance Sensor Description and Calibration

A wide angle distance sensor (Sharp) measured the linear distance between the submarine traverse and the motorized traverse. The measurement of this distance is required to control the motorized traverse drive as described in section 3.4.3 and is used indirectly to calculate the submarine velocity. The proximity detector is a optoelectronic device that emits an infrared beam and utilizes the reflection from the detected target to produce a nonlinear voltage output with respect to distance. The operational range of the sensor is between 20 and 150 cm over a 25° field of view. The response time of the device is 16.5 ms. The sensor required a supply voltage, V_{cc} , of +5 V, which was delivered through a power line embedded in the 50 ft power cable that connects to the electrical box sensor power supply. Further details about the electrical box can be found in section 3.4.1. In order to filter distance sensor power, a bypass capacitor of 100 μF was inserted between V_{cc} and ground.

The proximity sensor is 55 mm in length, 20 mm in height, and 18 mm in depth. The sensor was screwed into an aluminum holder that was designed for the device. The holder was clamped in place to the submarine traverse and positioned such that the infrared beam would strike a flat white piece of cardboard that was taped to the motorized traverse.

The distance sensor was calibrated by keeping the submarine traverse fixed and moving the motorized traverse by 1 cm increments. The change in distance of the motorized traverse was recorded using the facility control panel display. The voltage output from the sensor was sent to the National Instruments data acquisition box through a serial cable and was recorded by the Submarine DAQ software (3.4.1). The distance sensor output was recorded from a distance range of 16 +/- 1

cm to 140 +/- 1 cm. A 6th-order polynomial equation was fit to the data. See figure 3.6.

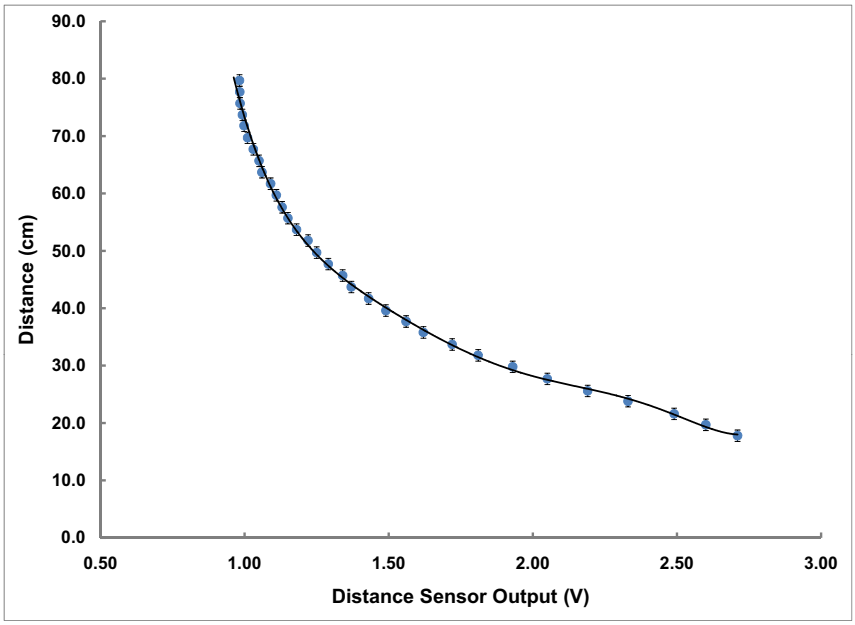

Figure 3.6. Plot of distance sensor calibration.

The relationship between distance and output voltage is nonlinear. There is a greater change or sensitivity in output at smaller distances. As the distance increases past 60 cm, the sensitivity is greatly reduced. Thus the motorized traverse was set to track the submarine traverse at a fixed distance of 40 cm.

3.4.3 System Control and Automation

The motorized traverse control panel accepts an analog control signal. The signal is output from the data acquisition box via 26 gauge wire and connected to the motorized traverse control panel via screw terminals. The motorized traverse control panel accepts a 0 to 10 V signal with 0 V halting the motorized traverse and 10 V accelerating the motorized traverse to maximum speed.

The Traverse Controller was implemented using LabVIEW 8.5. It is responsible for controlling the motorized traverse drive such that the motorized traverse tracks the submarine traverse at a

user specified distance. To accomplish this, the Traverse Controller uses the proportional-integral or PI control loop feedback mechanism. This application is composed of two VIs. The first VI implements the application's state machine as depicted in the flow chart in Appendix B. The second VI implements the PI control feedback mechanism.

The traverse controller user interface displays the PI algorithm parameters, the current distance sensor reading, the target motorized traverse to submarine traverse distance and charts the motorized traverse drive signal as shown in figure 3.7. Two buttons allow overriding of the motorized traverse drive value. The "Fixed Speed" button sets the motorized traverse drive signal to 2.5 V. This is a safe, moderate speed useful when relocating the motorized traverse along the water tunnel to prepare for an experiment. The "Stop Traverse" button sets the motorized traverse drive signal to 0 V and effectively stops the motorized traverse. The Stop button is used to shut down the application.

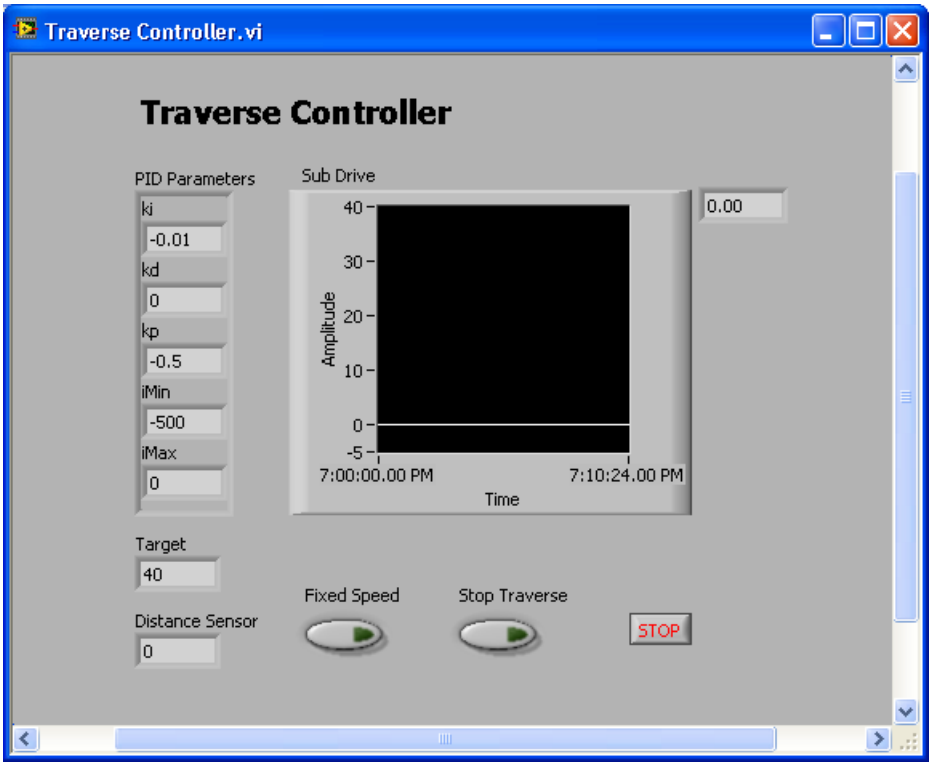

Figure 3.7. Screenshot of the Traverse Controller user interface.

The traverse controller is implemented using a state machine of three states. This application starts in the Initialize state where the PI control state is initialized. The next state is Run. This

state applies the PI control algorithm. First the current distance sensor value is received from the Submarine DAQ via a shared variable. This value is then fed into the PI algorithm. The PI algorithm output is limit checked into the valid motorized traverse drive signal range of 0 to 10 V. This value is then transmitted back to the Submarine DAQ via a second shared variable. The final state, Quit, is only executed if the user selects the Stop button. The state machine is halted and the application shuts down if this state is called. The PI algorithm uses the following internal equations:

$$SP - PV = e, \tag{3.1}$$

$$e \times K_p = P_{out}, \tag{3.2}$$

$$e + I_{state_1} = I_{state_2}, \tag{3.3}$$

$$I_{state_2} \times K_i = I_{out}, \tag{3.4}$$

$$P_{out} + I_{out} = MV, \tag{3.5}$$

where SP is the setpoint or, in this case, the desired tracking distance between the motorized traverse and the submarine traverse. PV is the processed variable or, in this case, the distance between the motorized traverse and the submarine traverse as measured by the distance sensor. The difference between these two values produces the error, e. The error multiplied by the proportional coefficient, K_p, leads to the proportional term, P_{out}. The error added to the integral state, I_{state_1}, produces the new integral state, I_{state_2}. This value is limit checked to lie within I_{min} to I_{max} inclusive to prevent the integral state from attaining values of extremely large magnitude. In the next iteration of the control algorithm, I_{state_2} will be used in place of I_{state_1}. The new integral state multiplied

Table 3.1. PI feedback control parameters

K_p	-0.5
K_i	-0.01
I_{max}	0
I_{min}	-500
SP	40

by the integral coefficient, K_i, produces the integral term, I_{out}. Adding P_{out} to I_{out} produces the manipulated variable MV or, in this case, the motorized traverse drive. Table 3.1 summarizes the PI parameters used.

3.4.4 LDV Measurements

Laser Doppler velocimetry (LDV) is a single point optical measuring technique which enables the velocity of seeded particles conveyed by a fluid flow to be measured in an unintrusive manner and is used to measure the velocity profile of the jet during self-propulsion. This technique was first reported by Yeh and Cummins (1964). See also Albrecht et al. (2003).

The LDV system consists of highly coherent light split into 2 beams and sent through a transmitter which crosses the beam in the probe volume to create a fixed interference pattern. As particles travel through the probe volume, they reflect light into a receiver when it crosses a region of constructive interference.

The tunnel was seeded with 13 μm diameter silver-coated glass hollow spheres to increase the number of particles that pass through the probe volume. Optics in the receiver allow the reflected light to focus onto an active area of an ultrafast photodiode. As seen by the photodetector, the light signal is a sinusoid modified by a Gaussian envelope. The sinusoid is isolated by a band-pass frequency filter. The frequency, f, of the sinusoid is typically measured using a Fast Fourier Transform. Since the fringe spacing in the interference pattern is known from calibration, thus, the speed of the particle can be calculated as follows:

$$Speed = fringe\ spacing \times f. \tag{3.6}$$

A one-component miniature laser Doppler velocimeter system (Measurement Science Enterprise miniLDV) was used in the experiments. The miniLDV is able to capture velocity measurements in the range of 1 to 300 m/s. The repeatability uncertainty is 0.1% with a typical accuracy of 99.7%. The probe must be rotated to measure multiple components of velocity.

An aluminum probe strut was designed to mount the miniLDV in a probe holder as shown in figure 3.8. The probe strut was attached to a 100 mm translational stage, thus allowing the miniLDV to translate in the vertical direction. The vertical stage was then mounted to a second 100 mm stage through a 90^o bracket plate. The second traverse allowed for translation of the probe in the horizontal direction. Software provided by Measurement Science Enterprise allowed for control of the motorized stages. The horizontal stage was attached to the traverse of the vehicle using eight 8-32 screws. The miniLDV probe volume was situated 0.5 inches away from the jet exit, or 0.25 jet diameters downstream. The probe volume was aligned so that the origin was referenced from the center of the jet.

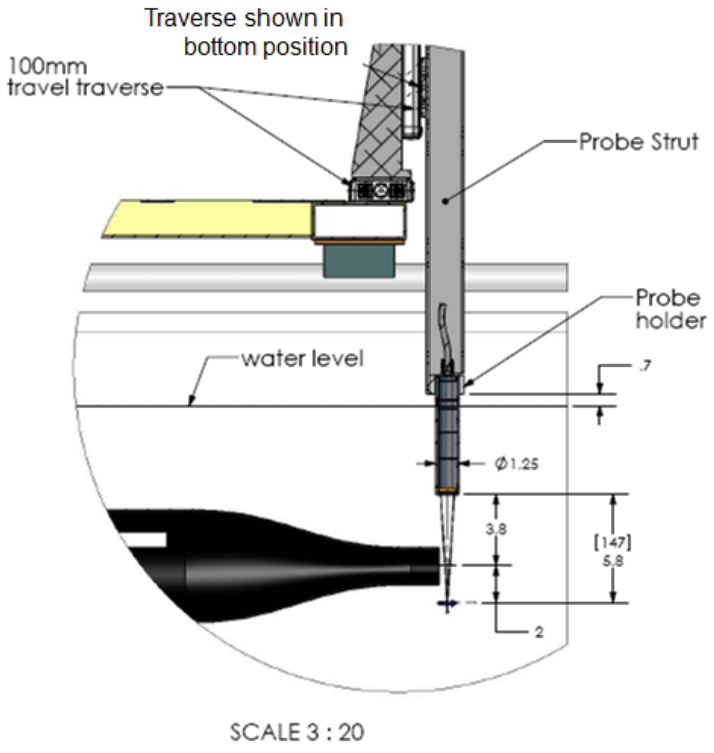

Figure 3.8. Schematic of LDV assembly mounted to the traverse of the vehicle.

The miniLDV system consists of the miniLDV probe, Processing Engine, and the 1D Burst Processor Acquisition Manager software package. The Processing Engine combines driver electronics, a band-pass filter, and a PCI acquisition card into one device, providing a USB 2.0 connection to the host computer and the Burst Processor Acquisition Manager software. The Burst Processor software collects data, moves the probe using the electronic traverses and presents flow statistics.

In initial propulsive efficiency experiments, a prototype of the modeled probe was used. This model was not capable of supporting a digital band-pass filter, so an analog band-pass filter was used in conjunction with the processing engine. Depending on the jet speed, the high-pass and low-pass filter settings were manually adjusted. For the self-propulsion experiments, the Doppler frequency of the jet ranged from 160 to 225 kHz. Within this speed range, the high-pass filter was set to 75 kHz and the low-pass filter was set to 100 kHz. The signal was amplified by adjusting the gain to a value of 20, and the minimal acceptable signal-to-noise ratio was set to a value of 3. The fringe spacing of this probe was 8.56 μm.

The second propulsive efficiency studies, along with the entrainment studies, were conducted using a later model of the miniLDV with a fringe spacing of 5.42 μm. The Processing Engine for this probe included the built-in digital filter. The following parameters were set for data acquisition using the Burst Processor Acquisition software: decimation, number of fast Fourier transform (FFT) points, threshold, minimum speed, maximum speed, minimum signal-to-noise ratio, and signal width. These parameters were adjusted depending on the speed of the fluid flow and which component of velocity was being measured. The decimation parameter adjusts the equivalent digitization rate of the hardware. The analog-to-digital converter hardware has a maximum digitization rate of 25 MHz. For lower frequency signals, a higher decimation parameter was used. The Doppler frequency of the signal is obtained by performing a FFT of the signal. As the number of FFT points increases there is a corresponding increase in the resolution of the results. Typically this was set to a value of 1024 or 512. The threshold parameter determines the processor signal trigger and was set slightly above the noise level. The minimal acceptable signal-to-noise ratio was set to a value of 4 for all experiments. Setting the signal width parameter allows for processing optimization of the entire

Doppler burst and was set to a value of "typical."

For LDV experiments, the water tunnel was seeded with neutrally buoyant, silver-coated hollow glass spheres with a 13 μm diameter and density of 1.6 g/cm^3 (Potters Industries) to increase the number of particles passing through the probe volume, hence increasing the data acquisition rate. Plastic barriers were used to confine the test section to 30 m in length, thus reducing the need to fill the entire tunnel with particles. The Processing Engine was mounted on the motorized traverse and was connected via USB to a computer located on the traverse. The Burst Processor software parameters were set by a remote connection from the water tunnel computer. The water tunnel computer was used to run the LabVIEW data acquisition software in conjunction with the traverse controller software.

Temporal data of the speed at the jet center located 0.25 jet diameters downstream was obtained using LDV. The Fast Fourier Transform (FFT) was calculated to determine if the pulsing frequency was distinguishable at various motor speeds for the pulsed jet configuration. Figure 3.9 shows the FFT results obtained for two different motor speeds. The predominant frequency determined through FFT at the lower motor speed was 2.36 Hz. The pulsing frequency as determined from the measurement of the rotational speed of the inner rotating shell was 2.3 +/- 0.1 Hz. The predominant frequency obtained through FFT of the jet speed correlates to the pulsing frequency at low motor speeds. As the motor speed increases, the predominant frequency as determined from the FFT is not as clearly defined. There appears to be a maximum peak at 8.4 Hz. Other peaks are present at 5.3, 6.4 and 9.9 Hz which are near in amplitude to the maximum peak. The pulsing frequency as determined from the measurement of the rotational speed of the inner rotating shell was 9.3 +/- 0.1 Hz, which is close to the predominant frequency. The pulsing frequency may be more clearly evident in the jet wake by modifying the location of the LDV probe volume to measure other axial and radial positions. It was shown in figure 4.6 that pulsing was clearly evident outside the diameter of the jet, denoted by dark regions in between jet pulses. LDV measurements of the jet speed within these regions may exhibit more clearly defined predominant frequencies in the FFT analysis.

3.4.5 Drag Measurements

Drag experiments were conducted to allow for measurements of the total hydrodynamic efficiency. Further details are discussed in section 4.4.3. Drag measurements of the submarine traverse, both with and without the vehicle, were obtained using a miniature precision load cell (Omega). The load cell was designed to measure both tension or compression loads with a 5 lb capacity. To minimize the effects of off-axis loads, the load cell uses a stainless steel weld construction. The accuracy of the device is +/- 0.15% of the full scale (linearity and hysteresis). The maximum output of the load cell is 10 mV without amplification. The load cell required a 5 VDC power input and was supplied by an AC powered signal conditioner (Omega Bridgesensor). The signal conditioner contains a precision differential instrumentation amplifier with voltage output. The frequency response of the device is 2 kHz with a gain range of 40 to 250. The excitation voltage supply range is 4 to 15 VDC, and was set to supply the necessary 5 VDC for the load cell. The output of the load cell was amplified by compressing the load cell by a known weight, near 100% of the full scale, and adjusting a potentiometer to achieve the desired full scale output. The load cell was then calibrated under compression by applying a series of known weights and measuring the amplified voltage output with a digital multimeter. The following curve was obtained as shown in figure 3.10. The output displays a linear relationship with applied load as expected.

3.4.5.1 Measurement Procedure

After calibration the load cell was placed in an assembly allowing the device to measure compression loads during the drag experiments. The load cell was anchored between the motorized traverse and submarine traverse. The active side of the load cell was screwed into a rod with a swivel bearing on the other end. This swivel bearing design relieved off-axis loads due to possible misalignment. The bearing was attached to an aluminum holder which was screwed into the submarine traverse by two 10-32 screws. See figure 3.11. An image of the drag experimental setup is shown in figure 3.12.

The drag force of the system was measured by setting the speed of the motorized traverse, allowing the load cell to compress and subsequently push the traverse with the attached submarine.

The experiments were then repeated without the submarine attached to measure the force necessary to push the traverse. The amplified load cell output was sent to the National Instruments data acquisition box and LabVIEW software was used to record the output. The Traverse Monitor software, as discussed in section 3.4.2.1, measured and recorded the motorized traverse speed and position. The friction force varied along the rails as they are not perfectly aligned. Data was recorded at the same start and stop position along the flume rails for each trial.

3.4.5.2 Calibration of Speed versus Drag Force

During self-propulsion experiments, the speed of the vehicle ranged from 8 to 55 cm/s. The drag on traverse both with and without the submarine was measured from speeds ranging from 8 to 60 cm/s. Figure 3.13 shows the relationship between drag force and speed. As speed increases, the drag of the traverse both with and without the submarine increases. The relationship between the traverse drag and speed is approximately linear. The force required to move the submarine traverse without attached submarine is the dominant contributor to the total drag on the system. On average, 89% of combined drag was due to friction in the submarine traverse. At lower speeds, the submarine traverse drag is as high as 96% of the combined drag. An estimate of the drag on the vehicle was obtained by subtracting the submarine traverse drag from the combined drag. The drag force on the submarine traverse increased at a higher rate with vehicle speed in comparison to the drag force on the vehicle itself. Due to magnitude of the uncertainty in the measurement of drag on the vehicle, it is not apparent that the drag on the vehicle is U_v^2.

A summary of the drag results for the traverse both with and without the vehicle attached is shown in Appendix D. Also shown in both summary tables is the standard deviation in the measurement of the drag force, σ_{drag}, and speed, σ_{speed}. The percent contribution of σ_{speed} to speed is greatest at the lower speed range for both cases as illustrated in figure 3.13.

3.4.5.3 Discussion of Spatial Variation of Drag Force Along Flume Rails

In general, as the speed increases the standard deviation in the drag force, σ_{drag}, increases. See figure 3.13. During drag experiments for the combined system, the percent contribution of σ_{drag} to the drag force reaches 26% in the lower-speed range in comparison to 17% in the higher-speed range. For the drag experiments of the traverse only, the percentage range is lower. The contribution reaches 24% at lower speeds and 14% at higher speeds. The variability in the drag measurement is a result of the misalignment of the flume rails. This misalignment increases the drag force on the submarine traverse pillowblocks. Figure 3.14 illustrates the variation of the drag force along the flume rails from a position of 0 to 700 cm as measured from the control panel.

Two cases are shown in the figure. One is at the low speed of 10.2 cm/s and another at a higher speed of 60.1 cm/s. Both of these cases are for combined system drag measurements. Although the measured drag is different for both cases, the dynamics of the measurements are similar. Both cases have peaks or increases in drag at similar positions along the flume rails. Given that the drag force varies along the rails, the experiments used the same start position.

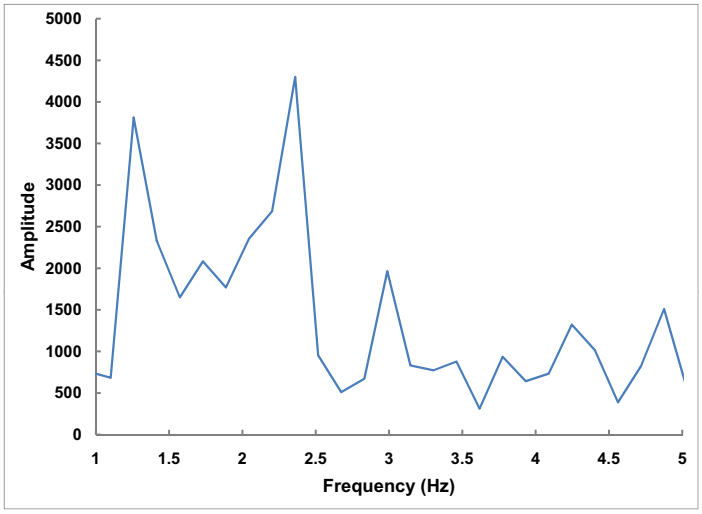

(a) FFT of jet center speed at a pulsing frequency of 2.3 Hz.

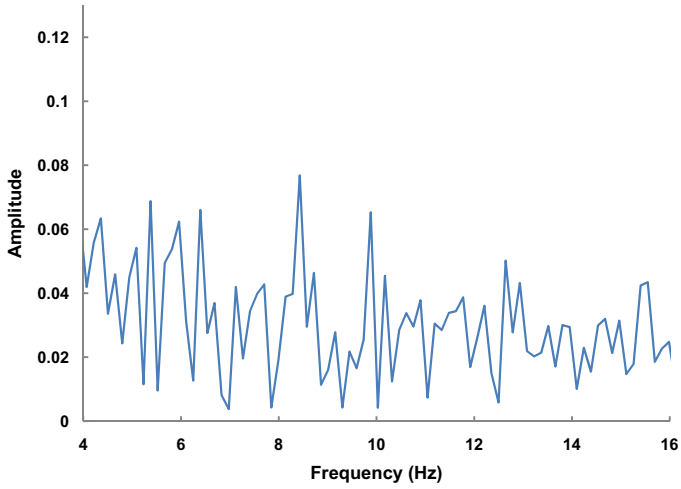

(b) FFT of jet center speed at a pulsing frequency of 9.3 Hz.

Figure 3.9. FFT of jet center speed at two pulsing frequencies. Pulsing frequency is distinguishable at the low motor speed.

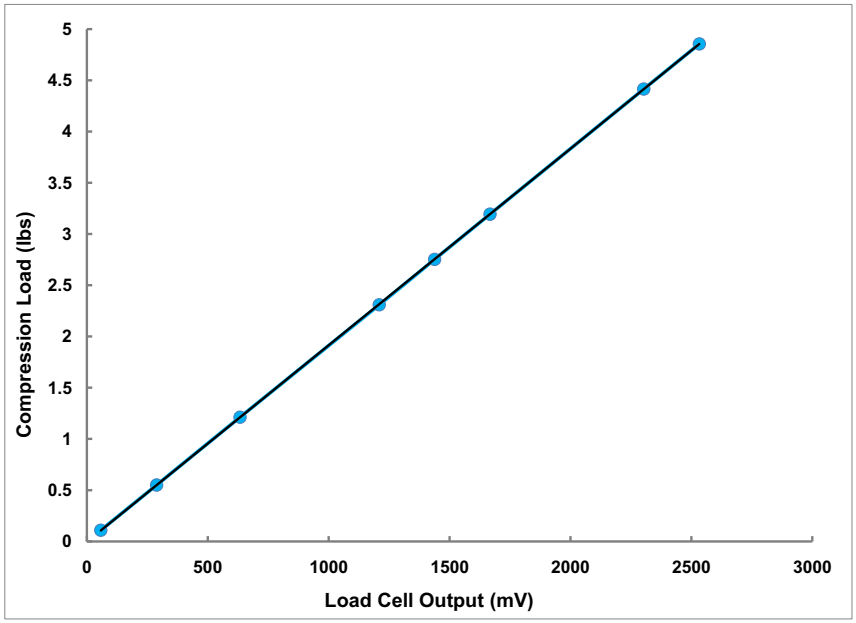

Figure 3.10. Load cell calibration under compression, y = 0.0019x − 0.003.

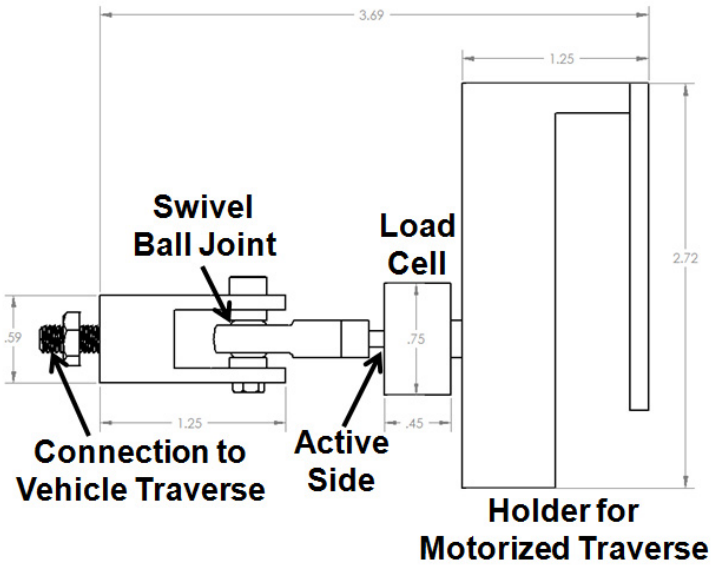

Figure 3.11. Schematic of load cell assembly.

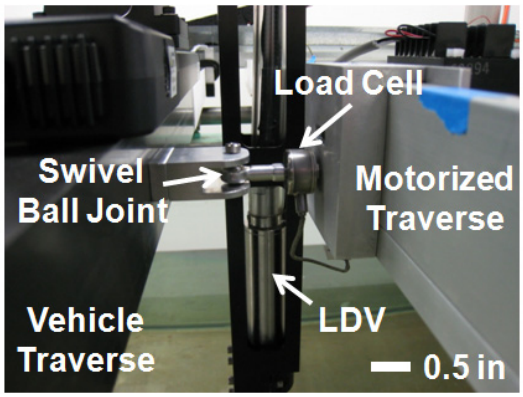

Figure 3.12. Image of load cell in drag experimental setup.

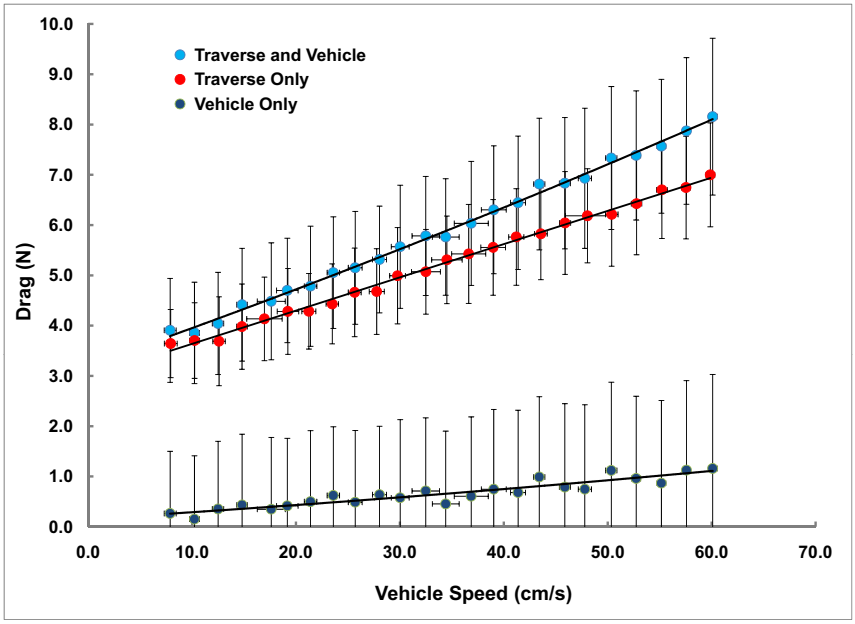

Figure 3.13. Drag measurements of traverse both with and without vehicle.

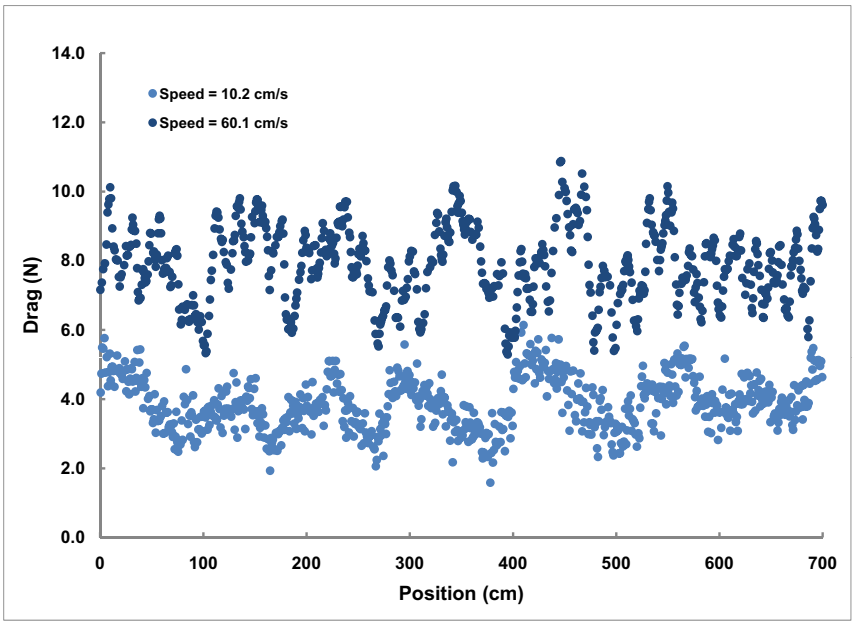

Figure 3.14. Graph illustrating the variation of the drag force along the flume rails.